Dual Origin of Room Temperature Sub-Terahertz Photoresponse in Graphene Field Effect Transistors

DOI:
10.1063/1.5018151

Document Version
Accepted author manuscript

Dual Origin of Room Temperature Sub-Terahertz Photoresponse in Graphene Field Effect Transistors

D.A. Bandurin,[1] I. Gayduchencko,[2,3] Y. Cao,[1] M. Moskotin,[4] A. Principi,[1] I.V. Grigorieva,[1] G. Goltsman,[2] G. Fedorov,[5] and D. Svintsov[5]

[1)] *School of Physics and Astronomy, University of Manchester, Manchester, M13 9PL, UK*

[2)] *Physics Department, Moscow State University of Education (MSPU),Moscow, 119435, Russian Federation*

[3)] *National Research Center Kurchatov Institute, Moscow, 123182, Russia*

[4)] *National Research University of Electronic Technology, 1, Shokin Square, Zelenograd, Moscow, 124498, Russia*

[5)] *Moscow Institute of Physics and Technology (State University), Dolgoprudny 141700, Russia*

Graphene is considered as a promising platform for detectors of high-frequency radiation up to the terahertz (THz) range due to graphene′s superior electron mobility. Previously it has been shown that graphene field effect transistors (FETs) exhibit room temperature broadband photoresponse to incoming THz radiation thanks to the thermoelectric and/or plasma wave rectification. Both effects exhibit similar functional dependences on the gate voltage and therefore it was found to be difficult to disentangle these contributions in the previous studies. In this letter, we report on combined experimental and theoretical studies of sub-THz response in graphene field-effect transistors analyzed at different temperatures. This temperature-dependent study allowed us to reveal the role of photo-thermoelectric effect, p-n junction rectification, and plasmonic rectification in the sub-THz photoresponse of graphene FETs.

Over the last decade, graphene has attracted a considerable attention in the fields of photonics[1] and optoelectronics[2]. The interest is motivated by graphenes unique gate-tuneable physical properties that allow realization of radiation detectors operating in a wide range of frequencies[3–6].

Electromagnetic radiation in the terahertz (THz) range deserves a special attention as it allows fast and non-destructive imaging of objects with a strong potential in medical and security sectors[7]. With this potential, the development of efficient THz generators and sensitive detectors is an important technological problem.

Recently, it has been shown that graphene field-effect transistors (FETs) can act as THz detectors exhibiting a dc photoresponse to impinging radiation[6,8–13]. A broadband photodetection in the sub-THz range with the responsivity reaching tens of V/W and noise equivalent power of hundreds of pW/Hz$^{1/2}$ has been demonstrated in graphene FETs designed in the configuration where the incoming radiation is coupled between the source and the gate terminals[8,9,12]. In this configuration, the photoresponse is usually attributed to the so-called Dyakonov-Shur (DS) rectification arising as a result of the plasma waves excitation in the FET channel[14,15]. However, other effects can also impact the photoresponse. For instance, photo-thermoelectric effect (PTE) arising from the temperature gradient in a FET can provide an additional rectification of the incoming high-frequency signal[4,6]. As we show below, both PTE and DS effects exhibit similar functional dependence on the gate voltage and result in the same sign of the photoresponse, that makes it challenging to point to the origin of the observed rectification. Further improvement of graphene-based THz photodetectors requires a deeper understanding of the rectification mechanisms governing the photoresponse.

In this work, we analyze the sub-THz photoresponse of graphene-based FET by comparing its responsivity at liquid nitrogen and room temperatures. Such temperature-dependent measurements allowed us to point to the effects arising from the heating of electronic system, overdamped plasma wave photodetection, and diode rectification. In particular, we show that the opposite sign of the Seebeck coefficients in the p-doped graphene channel and n-doped graphene in the vicinity of the metal contacts causes a significant PTE photoresponse to incoming radiation. When graphene channel is uniformly n-doped we observe an enhancement of the photoresponsivity with increasing temperature that can be explained by the overdamped DS scenario.

Our FET was made of graphene encapsulated between two slabs (50 nm thick each) of hexagonal boron nitride (hBN) by the dry-transfer method as described in Supplementary Material and elsewhere[16]. The FET was made in a dual-gated configuration such that the carrier density n in the channel was controlled by the global back gate electrode (located at a distance $d = 500$ nm) whereas the top-gate as well as the source terminals were extended to a millimeter scale and served as sleeves of a logarithmic spiral broadband antenna, see Fig. 1a-b and Supplementary Material.

Photoresponse measurements were performed in a variable temperature optical cryostat allowing coupling of the device under study to electromagnetic radiation via a polyethylene window. A silicon hemispherical lens focusing the incoming radiation to the device antenna was attached to the bottom of the device. The radiation was further funneled into the channel of our FET by its cou-

pling to the source and the top gate electrodes yielding the modulation of the top gate-to-channel voltage difference, Fig. 1a. The sub-THz radiation was generated by two backward wave oscillators allowing us to tune the frequency between $f = 0.13$ THz and 0.45 GHz. The power delivered to the device was measured using the Golay cell and recalculated accounting for the losses and size of the cryostat optical window and silicon lens[17].

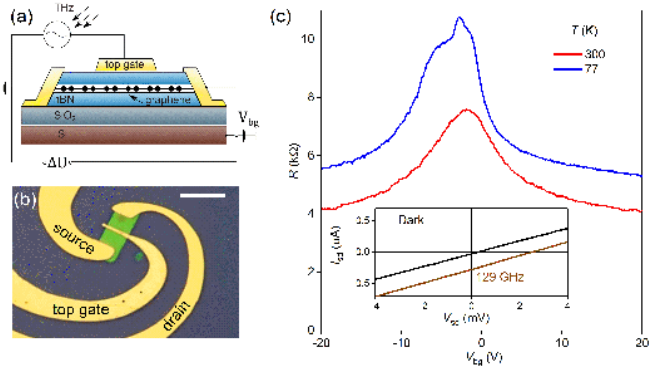

FIG. 1. (a) Schematics of a dual-gated graphene-based field effect transistor (b) An optical micrograph of our device. Scale bar is 6 μm (c) Two-terminal resistance as a function of V_{bg} measured at $T = 77$ K and 300 K. Inset: examples of the $I(V)-$ curves measured in the dark and under illumination with 0.13 THz. $V_{bg} = -20$ V, $T = 300$ K.

Prior to photoresponse measurements, we characterized the transport properties of our graphene FET. Figure 1c shows a two-terminal resistance R as a function of back gate voltage V_{bg} measured at $T = 77$ and 300 K. At RT, R exhibits a peak of 7 kΩ located around $V_{bg} = -2$ V corresponding to the charge neutrality point (CNP). Away from the CNP, R remains above several kΩ. At lower T, we observed an increase of the device resistance. Such behavior is opposite to that expected for doped graphene. This is not surprising as all our measurements were carried out in a two-terminal geometry and, therefore, R also accounts for a temperature-dependent contact resistance. For the same reason, the RT field effect mobility μ, extracted from the slope of $R(V_{bg})$ dependence, of our graphene device was only of 3.2×10^3 cm^{2}V^{-1}s^{-1}: two-terminal measurements provide the lower bound for μ, the latter is usually higher in encapsulated samples[?] . Nevertheless, at liquid nitrogen temperature we observed a two-fold increase of μ indicating the suppression of electron-phonon scattering leading to the increase of the scattering time τ.

The inset to Fig. 1c provides examples of the RT $I(V)$-curves of our photodetector measured in the absence (black) and in the presence of incoming radiation (brown). Both curves demonstrate linear dependence of the source-drain current I_{SD} on the bias voltage V_{SD}. The $I(V)$-curve measured under illumination is notably shifted to the right from the origin so that it intercepts the zero-current level at $\Delta U \approx 2.8$ mV, which we further refer to as the photovoltage.

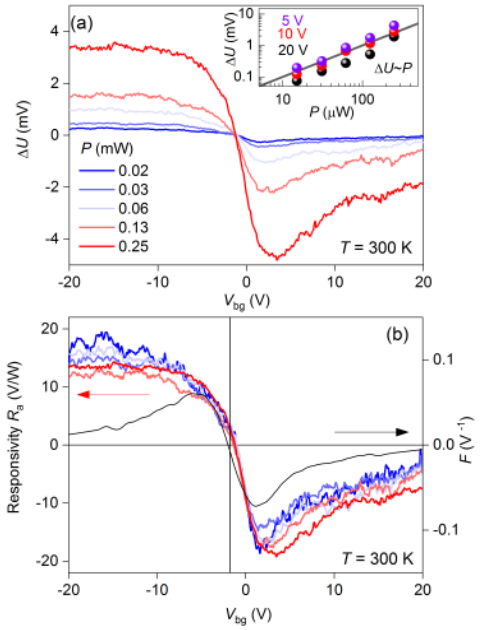

FIG. 2. (a) Photovoltage as a function of V_{bg} measured at varying power of incoming 0.13 THz radiation. $T = 300$ K. Inset: Photoresponse as a function of incoming power for different V_{bg}. The solid grey line represents $\Delta U \propto P$ scaling. (b) RT responsivity versus back gate voltage for different P. Black: Gate dependence of room-temperature FET-factor $F = -\sigma^{-1} d\sigma/dV_{bg}$, where σ is the channel conductance.

Figure 2a shows the results of the RT measurements of ΔU as a function of V_{bg} acquired at different power P of incoming 0.13 THz radiation. A finite ΔU is observed at all experimentally accessible V_{bg} except CNP where the sign of the photoresponse changes in agreement with ambipolar transport in graphene. The detected signal is highly asymmetric with respect to V_{bg}, such that it tends to zero at large positive V_{bg}, whereas it remains nearly constant with decreasing V_{bg} below CNP.

As the power of impinging radiation changes, the photoresponse voltage scales linearly with P, as shown in Fig. 2a. In Fig. 2b we plot the photoresponsivity $R_a = \Delta U/P$ as a function of V_{bg} corresponding to ΔU shown in Fig. 2a. All the dependences fall onto the same line and do not depend on the power of incoming radiation indicating that the device remains in the linear-response regime for the experimentally accessible power-range. The maximum value of R_a and the minimum noise equivalent power, NEP, of our device were 20 V/W and 0.6 nW/Hz$^{1/2}$ (see Supplementary Material) respectively that is comparable to the performance reported previously[8,9,12]. For further characterization of our photodetector, we have also measured its responsivity at higher frequencies and found that our device exhibits a broadband photoresponse at all experimentally accessible gate voltages away from the CNP. The results of such measurements are presented in Supplementary Material.

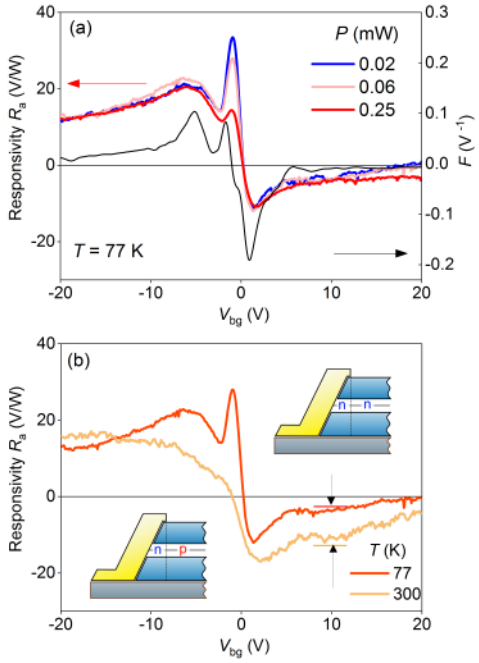

FIG. 3. (a) Responsivity as a function of V_{bg} measured at $T = 77$ K for different power of incoming 0.13 THz radiation (b) $R_a(V_{bg})$ at different temperatures measured at $P = 0.06$ mW. Arrows indicate the difference in R_a between the data acquired at $T = 77$ and 300 K

Figure 3a shows the responsivity as a function of V_{bg} measured at $T = 77$ K for varying power of incoming radiation. Similarly to the RT measurements, R_a is highly asymmetric with respect to positive and negative gate voltages. The photoresponse measured away from the CNP on a hole-doping side exhibits power-independent R_a slowly varying with V_{bg}. For n-doping, R_a rapidly tends to zero with increasing V_{bg}. Interestingly, at positive V_{bg}, the responsivity measured at $T = 77$ K was found to be smaller than that obtained at RT, Fig. 3b.

The gate dependence of R_a at 77 K peaks slightly to the left from the CNP, and for the lowest power of radiation reaches 30 V/W. In this gate voltage range, the $R(V_{bg})$ dependence can be represented as a superposition of two bell-shaped curves. Usually, such a double-peak structure of the $R(V_{bg})$ dependence is caused by the p-n junction formed at the boundaries between the regions with slightly different doping. In our device, those regions correspond to the areas not covered by the top-gate and the part of graphene under the top-gate in which a build-in electric field produces an unintentional doping. Thus, the spike in R_a can be attributed to the rectification of the high-frequency signal by this p-n junction[18]. The peak disappears with increasing P which is in agreement with p-n junction rectification scenario, as hot electrons pass over the junction barrier freely which suppresses rectification.

Further improvement of the THz detection efficiency requires a deeper understanding of the possible photoresponse mechanisms in graphene FETs which we discuss in detail below. Since graphene is characterized by the large optical phonon energy, hot electrons created by the Joule heating can remain at a higher temperature than that of the lattice and therefore may affect the photoresponse by the PTE[3,4]. Due to the asymmetric design of the antenna (Supplementary Material), the high-frequency current flows predominantly between the source and the gate terminals. This leads to the asymmetric temperature distribution across the graphene channel. Therefore, the electron system in the vicinity of the source remains at a higher average temperature T_S compared to that near the drain T_D, as shown in Fig. 4a. For a uniformly doped channel, the emerging photovoltage is given by

$$\Delta U_{\rm PTE} = -\int S dT \approx S(T_S - T_D) \qquad (1)$$

where $S \propto T\sigma^{-1}d\sigma/dE_F$ is the Seebeck coefficient, σ is the conductivity of graphene and $d\sigma/dE_F$ is its derivative with respect to the Fermi energy E_F. Within a factor of a slowly varying function $dV_{bg}/dE_F \propto V_{bg}^{1/2}$, the Seebeck coefficient and therefore $\Delta U_{\rm PTE}$ depend on the ratio between the 2D channel transconductance and its conductivity which we further refer to as the FET factor $F = -\sigma^{-1}d\sigma/dV_{bg}$. In Figs. 2b and 3a we plot $F(V_{bg})$ obtained by numerical differentiation of the data in Fig. 1c. The experimental photoresponse follows $F(V_{bg})$ for positive gate voltages however strongly deviates from it when $V_{bg} < 0$.

This asymmetry can be understood within the PTE model by taking into account n-doping of graphene near the gold contacts[19,20]. Considering the piecewise distribution of the Seebeck coefficient, S_{cont} near the contacts and S_{ch} in the remaining part of the channel, as shown in Fig. 4a, one obtains a modified expression for $\Delta U_{\rm PTE}$:

$$\Delta U_{\rm PTE} = (S_{ch} - S_{cont})(T_S - T_D). \qquad (2)$$

Equation (2) readily explains the asymmetry of the detector characteristics $R_a(V_{bg})$ shown in Fig. 2b and 3a. Indeed, S_{ch} is controlled by the gate voltage and changes sign at the CNP while S_{cont} is dictated only by the built-in field at the graphene-metal interface. The n-doping of graphene by contacts[19,20] implies that $S_{cont} < 0$. This increases the absolute value of the photovoltage for p-doped channel and decreases it for n-doped . At high positive voltage $V_{bg} \geq 20$ V, the observed response approaches zero, which hints on the equal doping of channel and contacts. At this point, the electron Fermi energy in the channel is estimated as $E_F \approx \hbar v_F(\pi C_{bg}V_{vg})^{1/2} \approx 0.1$ eV (where v_F is the Fermi velocity and C_{bg} is the gate-to-channel capacitance), which is close to the value of contact doping at graphene/metal interface[21].

An alternative view on the photodetection processes in 2D FETs is the so-called DS scenario which predicts the rectification of the ac signal by the field effect and hydrodynamic nonlinearities possibly enhanced by the resonant

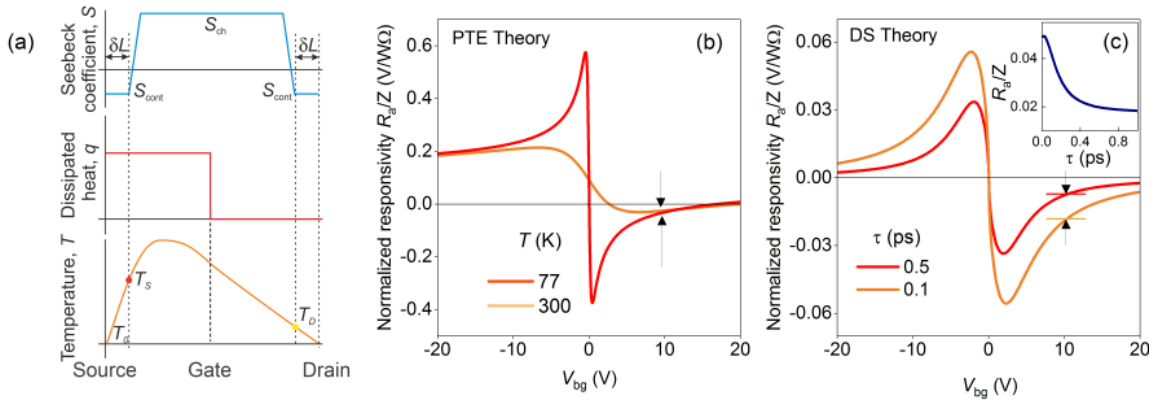

FIG. 4. (a) Distribution of the Seebeck coefficient S, dissipated heat q and temperature T in a FET with the radiation coupled between the source and gate terminals. (b) Normalized photo-thermoelectric responsivity as a function of V_{bg} calculated for $T = 77$ and 300 K. (c) Normalized DS photoresponsivity as a function of V_{bg} calculated with eq. (3) for given τ and $f = 0.13$ THz. Inset: R_a/Z as a function of τ calculated at $V_{bg} = -5$ V. $V_{bg} = 0$ V corresponds to the CNP.

plasma wave excitations[14]. Though the conditions of the hydrodynamic transport are usually fulfilled in encapsulated graphene[22,23], the plasmonic enhancement of the nonlinearities in our device looks hardly possible as the plasma waves are overdamped. Indeed, for our device, we estimate the scattering time with respect to momentum non-conserving collisions τ to hundreds of fs so that $\omega\tau < 1$, where $\omega = 2\pi f$. In this non-resonant regime, the DS photodetection yields a broadband photoresponse (also referred to as resistive self-mixing) with the photovoltage given by[8,14]:

$$\Delta U_{DS} = -\frac{U_a^2}{4}\frac{1}{\sigma}\frac{d\sigma}{dV_g}g(\omega) \propto F(V_g) \qquad (3)$$

where U_a is the ac gate-to-source voltage, L is the channel length, $g(\omega) = [\sinh^2 kL - \sin^2 kL]/[\sinh^2 kL + \cos^2 kL]$ is the form factor depending on the wave number $k = (\omega/2\tau)^{1/2}/s$ of the overdamped plasma wave, $s = \sqrt{e|V_{bg}|/m}$ is the plasma wave velocity, e is the electron charge, and m is the cyclotron mass of charge carriers. Importantly, ΔU_{DS} is also proportional to F, that makes it difficult to distinguish the PTE and DS mechanisms by studying the gate-voltage dependences only, see equations (1) and (3). We also emphasize, that these two mechanisms yield the same sign of the photovoltage (see Supplementary Material). As we show below, the role of each effect in the photovoltage can be revealed by studying the photoresponse at different temperatures.

We stat our analysis from the temperature dependence of the PTE. To this end, we express the electron temperature in eq. (2) through the incoming radiation power by solving the heat transfer equation (Supplementary Material). This results in the responsivity

$$R_a \approx \frac{3}{2\pi^2}\left[\frac{e}{k_B}(S_{cont} - S_{ch})\right]\frac{e|Z_{\text{eff}}|}{k_B T}\frac{\delta L}{L}, \qquad (4)$$

where Z_{eff} is the effective resistance relating the power impinging on the antenna with resulted gate-to-channel voltage, δL is the length of doped contact region and L is the overall channel length. In Fig. 4b we show the normalized responsivity $R_a/|Z_{\text{eff}}|$ as calculated from eq. (4) for different temperatures and realistic estimates of $\delta L = 100$ nm[24]. At negative V_{bg}, both curves saturate and exhibit temperature-independent response. When approaching the CNP from the p-doping side, one observes an increase in responsivity with lowering temperature. Both observations are in accordance with the experimental data for p-doped graphene shown in Fig. 3b. The model allows us to roughly estimate $|Z_{\text{eff}}| \approx 100$ Ω, which is close to that estimated from the equivalent circuit (see Supplementary Material).

Despite the agreement with data at negative gate voltages, the PTE theory does not provide a complete qualitative description of the experiment: in the n-doped regime, the absolute value of the RT responsivity is three times higher than that observed at $T = 77$ K which contradicts the PTE scenario, because the latter yields the decrease of the photovoltage with increasing temperature, Fig. 4b. Indeed, in the case of PTE, the relative heating $T_S - T_D$ is proportional to the dissipated heat $q = \sigma E^2/2$ and inversely proportional to the thermal conductance χ. At liquid nitrogen temperatures and away from CNP, the electric and thermal conductivity are coupled by the Wiedemann-Franz law, and therefore $T_S - T_D \propto q/\chi \propto T^{-1}$. Recalling that in the degenerate electron system the Seebeck coefficient grows linearly with T, one obtains the temperature independent ΔU_{PTE}. In the non-degenerate case S weakly depends on temperature while the relative heating and therefore ΔU_{PTE} drop upon increasing T. Further reduction of the photovoltage at elevated temperatures occurs due to electron-phonon cooling[25] and interaction with hyperbolic phonon-polaritons in hBN[26].

The increase of the responsivity in n-doped graphene at RT can be qualitatively explained by the broadband DS photodetection scenario. Indeed, although the eq. (3)

does not depend on temperature explicitly, the latter enters the expression for the plasma wave vector k through the temperature-dependent scattering rate τ[14]. The evaluation of the DS response with eq. (3) for $f = 0.13$ THz including the form factor $g(\omega)$ for different relaxation times demonstrates a counterintuitive increase in signal at shorter τ, as shown in Fig. 4c, that is in qualitative agreement with data in Fig. 3b. Previously, we mentioned that in our device the momentum relaxation time drops with increasing temperature (e.g. due to electron-phonon scattering). Moreover, the PTE response is expected to vanish for highly n-doped device (Fig. 4b). Therefore, an increase of the experimentally detected responsivity at RT may be caused by the overdamped DS photoresponse being the dominant photodetection mechanism. We also note that for an accurate evaluation of the DS photovoltage in such FET, one needs to account for its dual-gated design, that is the subject of our further studies.

In summary, we have demonstrated that FETs based on graphene encapsulated in hexagonal boron nitride can serve as high-responsivity sub-THz photodetectors with low NEP. We have shown, how the measurements of the photoresponse at different temperatures can provide the information on the rectification mechanisms governing the photoresponse. Namely, by comparing the photoresponse at different temperatures, we have found that the opposite sign of the Seebeck coefficients in the p-doped graphene channel and n-doped graphene-metal interface results in the significant PTE rectification of the high-frequency radiation. For a uniformly n-doped graphene (where the PTE is minimized), we have found that the photoresponse increases with increasing temperature that contradicts the PTE scenario and can be qualitatively explained by the overdamped plasma wave rectification being the dominant contribution to the photovoltage at RT. Furthemore, we have found that a p-n junction, formed in the channel of a FET, provides an additional rectification mechanism allowing one to increase the responsivity of graphene-based THz photodetectors.

SUPPLEMENTARY MATERIAL

See supplementary material for the details of the device fabrication, photoresponse measurements at various frequencies, measurements of the device noise equivalent power, the theoretical model describing photo-thermoelectric response.

ACKNOWLEDGEMENTS

D.A.B. acknowledges Leverhulme Trust for financial support. The work of DS was supported by the grant #16-19-10557 of the Russian Scientific Foundation. G.F.,I.G., M.M. and G.G acknowledge Russian Science Foundation (Grant No.14-19-01308, MIET and Grant No. 17-72-30036, MSPU), Ministry of Education and Science of the Russian Federation (contract No. 14.B25.31.0007 and Task No. 3.7328.2017/LS) and Russian Foundation for Basic Research (grant no. 15-02-07841). The authors are grateful to Prof. M.S. Shur for helpful discussions.

[1] F. Bonaccorso, Z. Sun, T. Hasan, and A. Ferrari, Nat. Photon. **4**, 611 (2010).
[2] F. Koppens, T. Mueller, P. Avouris, A. Ferrari, M. Vitiello, and M. Polini, Nat. Nanotechnol. **9**, 780 (2014).
[3] N. M. Gabor, J. C. W. Song, Q. Ma, N. L. Nair, T. Taychatanapat, K. Watanabe, T. Taniguchi, L. S. Levitov, and P. Jarillo-Herrero, Science **334**, 648 (2011).
[4] M. Jung, P. Rickhaus, S. Zihlmann, P. Makk, and C. Schnenberger, Nano Lett. **16**, 6988 (2016).
[5] J. Yan, M. H. Kim, J. A. Elle, A. B. Sushkov, G. S. Jenkins, H.-w. M. Milchberg, M. S. Fuhrer, and H. Drew, Nat. Nanotechnol. **7**, 472 (2012).
[6] X. Cai, A. B. Sushkov, R. J. Suess, M. M. Jadidi, G. S. Jenkins, L. O. Nyakiti, R. L. Myers-Ward, S. Li, J. Yan, D. K. Gaskill, *et al.*, Nat. Nanotechnol. **9**, 814 (2014).
[7] D. Mittleman, *Sensing with terahertz radiation*, Vol. 85 (Springer, 2013).
[8] L. Vicarelli, M. Vitiello, D. Coquillat, A. Lombardo, A. Ferrari, W. Knap, M. Polini, V. Pellegrini, and A. Tredicucci, Nat. Mater. **11**, 865 (2012).
[9] D. Spirito, D. Coquillat, S. L. D. Bonis, A. Lombardo, M. Bruna, A. C. Ferrari, V. Pellegrini, A. Tredicucci, W. Knap, and M. S. Vitiello, Appl. Phys. Lett. **104**, 061111 (2014).
[10] J. Tong, M. Muthee, S.-Y. Chen, S. K. Yngvesson, and J. Yan, Nano Lett. **15**, 5295 (2015).
[11] G. Auton, D. B. But, J. Zhang, E. Hill, D. Coquillat, C. Consejo, P. Nouvel, W. Knap, L. Varani, F. Teppe, J. Torres, and A. Song, Nano Lett. **17**, 7015 (2017).
[12] A. Zak, M. A. Andersson, M. Bauer, J. Matukas, A. Lisauskas, H. G. Roskos, and J. Stake, Nano Lett. **14**, 5834 (2014).
[13] H. Qin, J. Sun, S. Liang, X. Li, X. Yang, Z. He, C. Yu, and Z. Feng, Carbon **116**, 760 (2017).
[14] M. Dyakonov and M. Shur, IEEE Trans. El. Dev. **43**, 380 (1996).
[15] A. Tomadin and M. Polini, Phys. Rev. B **88**, 205426 (2013).
[16] A. Kretinin, Y. Cao, J. Tu, G. Yu, R. Jalil, K. Novoselov, S. Haigh, A. Gholinia, A. Mishchenko, M. Lozada, *et al.*, Nano Lett. **14**, 3270 (2014).
[17] G. Fedorov, A. Kardakova, I. Gayduchenko, I. Charayev, B. Voronov, M. Finkel, T. Klapwijk, S. Morozov, M. Presniakov, I. Bobrinetskiy, *et al.*, Appl. Phys. Lett. **103**, 181121 (2013).
[18] Y. B. Vasilyev, G. Y. Vasileva, S. Novikov, S. Tarasenko, S. Danilov, and S. Ganichev, arXiv preprint arXiv:1711.03803 (2017).
[19] R. Nouchi, T. Saito, and K. Tanigaki, Appl. Phys. Express **4**, 035101 (2011).
[20] K. McCreary, K. Pi, A. Swartz, W. Han, W. Bao, C. Lau, F. Guinea, M. Katsnelson, and R. Kawakami, Phys. Rev. B **81**, 115453 (2010).
[21] E. J. Lee, K. Balasubramanian, R. T. Weitz, M. Burghard, and K. Kern, Nat. Nanotechnol. **3**, 486 (2008).
[22] D. A. Bandurin, I. Torre, R. K. Kumar, M. Ben Shalom, A. Tomadin, A. Principi, G. H. Auton, E. Khestanova, K. S. Novoselov, I. V. Grigorieva, L. A. Ponomarenko, A. K. Geim, and M. Polini, Science **351**, 1055 (2016).
[23] R. Krishna Kumar, D. A. Bandurin, F. M. D. Pellegrino, Y. Cao, A. Principi, H. Guo, M. Auton, G. H. amd Ben Shalom, L. A. Ponomarenko, G. Falkovich, K. Watanabe, T. Taniguchi, I. V. Grigorieva, L. S. Levitov, M. Polini, and A. K. Geim, Nat. Phys. **13**, 1182 (2017).
[24] M. B. Shalom, M. Zhu, V. Falko, A. Mishchenko, A. Kretinin, K. Novoselov, C. Woods, K. Watanabe, T. Taniguchi, A. Geim, *et al.*, Nat. Phys. **12**, 318 (2016).
[25] J. Crossno, X. Liu, T. A. Ohki, P. Kim, and K. C. Fong, Appl. Phys. Lett. **106**, 023121 (2015).
[26] K. Tielrooij, N. Hesp, A. Principi, M. Lundeberg, E. Pogna, L. Banszerus, Z. Mics, M. Massicotte, P. Schmidt, D. Davydovskaya, *et al.*, Nat. Nanotechnol **13**, 41-46 (2018).